Human Molecular Genetics, 2010, Vol. 19, No. 7 ***1347–1357***
doi:10.1093/hmg/ddq011
Advance Access published on January 12, 2010

Activation of Rho GTPases in Smith–Lemli–Opitz syndrome: pathophysiological and clinical implications

Xiao-Sheng Jiang[1], Christopher A. Wassif[1], Peter S. Backlund[2], Li Song[1], Lynne A. Holtzclaw[3], Zheng Li[4], Alfred L. Yergey[2] and Forbes D. Porter[1,*]

[1]Section on Molecular Dysmorphology, Program in Developmental Endocrinology and Genetics, Eunice Kennedy Shriver National Institute of Child Health, [2]Section on Mass Spectrometry and Metabolism, Office of the Scientific Director, Eunice Kennedy Shriver National Institute of Child Health, [3]Section on Cell Biology and Signal Transduction, Program in Developmental Neuroscience, Eunice Kennedy Shriver National Institute of Child Health and [4]Unit on Synapse Development and Plasticity, Gene, Cognition and Psychosis Program, National Institute of Mental Health, National Institutes of Health, DHHS, Bethesda, MD 20892, USA

Received December 7, 2009; Revised January 5, 2010; Accepted January 11, 2010

Smith–Lemli–Opitz syndrome (SLOS) is a malformation syndrome with neurocognitive deficits due to mutations of *DHCR7* that impair the reduction of 7-dehydrocholesterol to cholesterol. To investigate the pathological processes underlying the neurocognitive deficits, we compared protein expression in *Dhcr7*$^{+/+}$ and *Dhcr7*$^{\Delta 3\text{-}5/\Delta 3\text{-}5}$ brain tissue. One of the proteins identified was cofilin-1, an actin depolymerizing factor which regulates neuronal dendrite and axon formation. Differential expression of cofilin-1 was due to increased phosphorylation. Phosphorylation of cofilin-1 is regulated by Rho GTPases through Rho-Rock-Limk-Cofilin-1 and Rac/Cdc42-Pak-Limk-Cofilin-1 pathways. Pull-down assays were used to demonstrate increased activation of RhoA, Rac1 and Cdc42 in *Dhcr7*$^{\Delta 3\text{-}5/\Delta 3\text{-}5}$ brains. Consistent with increased activation of these Rho GTPases, we observed increased phosphorylation of both Limk and Pak in mutant brain tissue. Altered Rho/Rac signaling impairs normal dendritic and axonal formation, and mutations in genes encoding regulators and effectors of the Rho GTPases underlie other human mental retardation syndromes. Thus, we hypothesized that aberrant activation of Rho/Rac could have functional consequences for dendrite and axonal growth. *In vitro* analysis of *Dhcr7*$^{\Delta 3\text{-}5/\Delta 3\text{-}5}$ hippocampal neurons demonstrated both axonal and dendritic abnormalities. Developmental abnormalities of neuronal process formation may contribute to the neurocognitive deficits found in SLOS and may represent a potential target for therapeutic intervention.

INTRODUCTION

Smith–Lemli–Opitz syndrome (SLOS, OMIM #270400) is the prototypical example of a human malformation syndrome due to an inborn error of cholesterol synthesis. Frequent findings in SLOS include a typical facial appearance (microcephaly, ptosis, a small upturned nose, micrognathia and cleft palate), limb anomalies (post-axial polydactyly and 2–3 toe syndactyly), genital anomalies (hypospadius and ambiguous genitalia), growth retardation, mental retardation, behavioral problems and autistic features (1). SLOS is an autosomal recessive disorder due to mutation of the 7-dehydrocholesterol reductase gene (*DHCR7*) (2–4). *DHCR7* maps to human chromosome 11q12–13 (3), and over 130 different mutations have been described (5,6). DHCR7 is an integral membrane protein that reduces the Δ7 bond in 7-dehydrocholesterol (7DHC) to yield cholesterol in the final step of the cholesterol synthetic pathway (Fig. 1A). Impaired DHCR7 activity results in the accumulation of precursor sterols, 7DHC, its isomer 8-dehydrocholesterol (8DHC), and a deficiency of cholesterol during embryonic development.

The pathological mechanisms underlying the malformations and clinical problems found in SLOS are diverse. This is due

*To whom correspondence should be addressed at: Section on Molecular Dysmorphology, PDGEN, NICHD, NIH, DHHS, Building 10, Room 9D42, 10 Center Drive, Bethesda, MD 20892, USA. Tel: +1 3014354432; Fax: +1 3014805791; Email: fdporter@mail.nih.gov

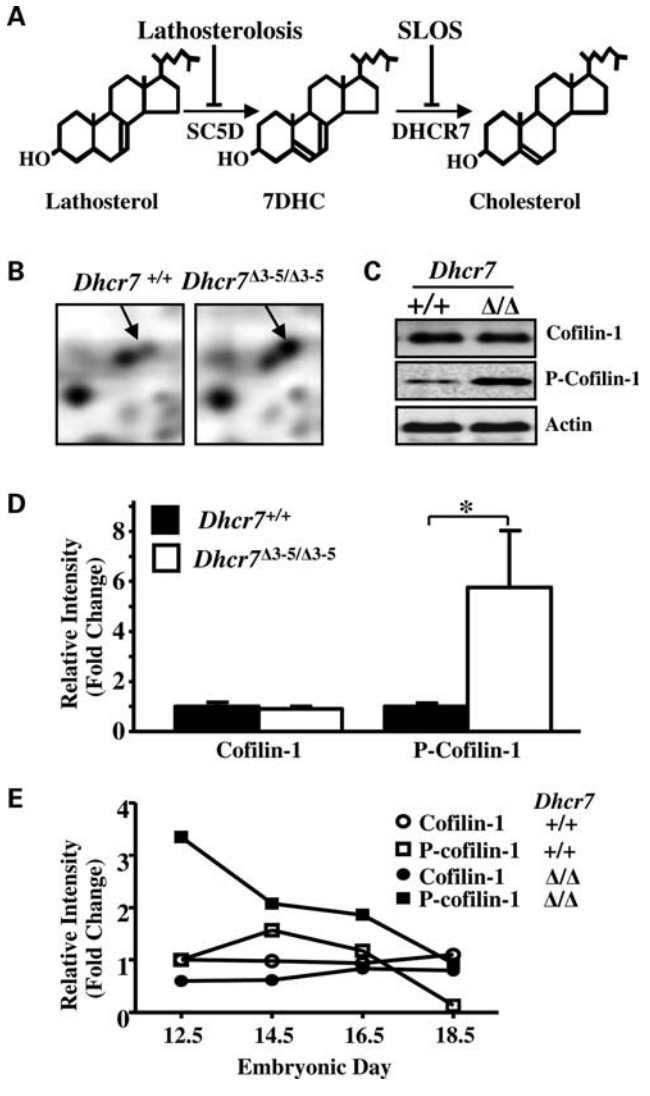

Figure 1. Increased phosphorylation of cofilin-1 in *Dhcr7*$^{\Delta 3\text{-}5/\Delta 3\text{-}5}$ brain tissue. (**A**) SLOS and lathosterolosis are, respectively, due to deficiency of 3β-hydroxysterol-Δ7-reductase (DHCR7) and lathosterol 5-desaturase (SC5D) activity. These enzymes function sequentially with SC5D converting lathosterol to 7DHC and DHCR7 reducing 7DHC to yield cholesterol. In mouse models corresponding to these two human malformation syndromes, there is a similar deficiency of cholesterol; however, 7DHC accumulates in SLOS and lathosterol accumulates in lathosterolosis. (**B**) Representative sections of silver-stained 2-DE gels comparing *Dhcr7*$^{+/+}$ and *Dhcr7*$^{\Delta 3\text{-}5/\Delta 3\text{-}5}$ mouse brain protein expression. The differentially expressed protein spot indicated by the arrow was found to contain cofilin-1. (**C**) Differential expression of cofilin-1 was validated by western blot. Comparing pooled *Dhcr7*$^{+/+}$ (+/+) and *Dhcr7*$^{\Delta 3\text{-}5/\Delta 3\text{-}5}$ (Δ/Δ) samples, we found that although total cofilin-1 expression was similar, P-cofilin-1 was markedly increased in E18.5 *Dhcr7*$^{\Delta 3\text{-}5/\Delta 3\text{-}5}$ brain tissue. Twenty micrograms of protein were loaded per lane and actin was used as a loading control. (**D**) Differential expression of P-cofilin-1 was quantified by comparison of five control (filled bars) and mutant (open bars) samples (mean ± SD, $^{*}P < 0.05$). (**E**) Cofilin-1 and P-cofilin-1 expression were evaluated through embryonic development. Values are relative to control levels at E12.5.

to the fact that cholesterol has multiple biological functions, and 7DHC is known to enter these various biological processes. Cholesterol is a major lipid component of cellular membranes and the altered sterol composition in SLOS affects the physiochemical properties and functions of cellular membranes. Synthetic membranes containing 7DHC have an atypical membrane organization (7), and 7DHC decreases membrane bending rigidity (8). Cholesterol is also a major component of lipid rafts. Lipid rafts are ordered lipid domains that function in signal transduction. Substitution of 7DHC for cholesterol alters both lipid raft stability (9) and protein composition (10). These physical perturbations of membrane structure likely underlie functional defects in IgE receptor mediated mast cell degranulation and cytokine production (11), NMDA receptor function (12) and serotonin$_{1A}$ receptor ligand binding (13). Cholesterol also plays a major role in embryonic development; it is necessary for the proper processing and function of the hedgehog family of morphogens (14). It is likely that both the cholesterol deficiency and accumulation of toxic levels of dehydrocholesterol or metabolites of dehydrocholesterol contribute to various pathological processes in SLOS.

We (12,15) and others (16) have previously reported the development of mouse models with SLOS. Mice homozygous for a null mutation of *Dhcr7* (*Dhcr7*$^{\Delta 3\text{-}5/\Delta 3\text{-}5}$) have a low frequency of cleft palate, demonstrate neurological problems and die soon after birth due to failure to feed (12). The lack of multiple major malformations is likely due to transfer of maternal cholesterol to the developing embryo (17,18). Biochemically, tissues from *Dhcr7*$^{\Delta 3\text{-}5/\Delta 3\text{-}5}$ embryos have significantly decreased cholesterol levels and markedly increased dehydrocholesterol levels. By embryonic day 18.5, 1 day prior to birth, 7DHC and 7-dehydrodemsosterol (a second sterol that accumulates in embryonic brain tissue) account for 70–75% of total sterols. Thus, these mice provide a model system in which it is possible to identify proteins whose expression are altered in SLOS brain tissue. We postulated that the identification of specific proteins with altered expression would give insight into biological processes that are perturbed in SLOS and contribute to its pathology. One of the proteins that we identified by quantitative proteomic analysis was cofilin-1. Specifically, we found increased phosphorylation of cofilin-1, which is an actin depolymerizing factor that regulates neuronal dendrite and axon formation (19). The activity of cofilin-1 is regulated by phosphorylation. Further analysis showed alterations in the Rho GTPase/Lim kinase regulatory cascade that regulates cofilin activity consistent with increased phospho-cofilin-1 (P-cofilin-1). Also consistent with our proteomic findings, functional characterization demonstrated altered levels of actin filament in *Dhcr7* mutant brain tissue and aberrant dendrite actin filament formation and abnormal dendrite/axon growth in *Dhcr7* mutant hippocampal neurons. Combined with previous work showing that mutations of genes involved in the Rho GTPase/Lim kinase regulatory cascade cause mental retardation (20,21), our current work suggests that altered Rho GTPase/Lim kinase/cofilin-1 function underlies some of the cognitive deficits found in SLOS.

RESULTS

Increased cofilin-1 phosphorylation in *Dhcr7*$^{\Delta 3\text{-}5/\Delta 3\text{-}5}$ brain tissue

In order to identify biological pathways that are altered in SLOS, we used proteomic techniques to identify differentially expressed proteins in *Dhcr7*$^{\Delta 3\text{-}5/\Delta 3\text{-}5}$ brain tissue. Total protein extracts were obtained from seven E18.5 *Dhcr7*$^{\Delta 3\text{-}5/\Delta 3\text{-}5}$

mutant embryos and seven *Dhcr7*$^{+/+}$ control embryos. Two-dimensional gel electrophoresis (2-DE) was used to separate proteins. Three replicate silver stained, two-dimensional gels were produced for both *Dhcr7*$^{+/+}$ and *Dhcr7*$^{\Delta 3\text{-}5/\Delta 3\text{-}5}$ total brain protein extracts. For comparison of total protein extracts from *Dhcr7*$^{+/+}$ and *Dhcr7*$^{\Delta 3\text{-}5/\Delta 3\text{-}5}$ brains, 1107 individual protein spots were quantified using PDQuest 8.0 software. Fifty-six (5.1%) of these protein spots were differentially expressed ($R \leq 0.83$ or $R \geq 1.20$, $P < 0.05$, unpublished data). Differentially expressed protein spots were excised from Coumassie blue stained preparative gels, and subjected to 'in-gel' digestion with trypsin. The resulting tryptic peptides were extracted and analyzed by a combination of high resolution MALDI tandem mass spectrometry and liquid chromatography/tandem mass spectrometry. MS/MS spectra from both instruments were analyzed and matched to protein sequences present in the Swiss-Prot database using the Mascot search program (22).

Figure 1B shows a portion of representative silver stained gels comparing proteins from *Dhcr7*$^{+/+}$ and *Dhcr7*$^{\Delta 3\text{-}5/\Delta 3\text{-}5}$ brains. Densitometric quantification of the indicated protein spot in three independent gels showed a 3.8-fold increase ($P = 0.005$) in mutant brain tissue compared with control brain tissue. Mass spectrometric analysis of this protein spot identified three peptides corresponding to cofilin-1 (Supplementary Material, Fig. S1). Western blot analysis was used to validate altered expression of cofilin-1 in *Dhcr7* mutant brains. Whereas total cofilin-1 levels did not appear to differ between *Dhcr7*$^{+/+}$ and *Dhcr7*$^{\Delta 3\text{-}5/\Delta 3\text{-}5}$ brains, levels of P-cofilin-1 were significantly increased in E18.5 *Dhcr7*$^{\Delta 3\text{-}5/\Delta 3\text{-}5}$ brain tissue compared with control brain tissue (Fig. 1C). Analysis of brain tissue from five individual mutant and control embryos (Fig. 1D) showed a 5.8-fold increase in P-cofilin-1 levels ($P = 0.02$), and confirmed no significant differences in total cofilin (phosphorylated and non-phosphorylated, $P = 0.30$). Cofilin-1 levels are relatively constant from E12.5 through E18.5, but P-cofilin-1 levels vary during development. However, P-cofilin-1 levels are elevated in *Dhcr7*$^{\Delta 3\text{-}5/\Delta 3\text{-}5}$ brain tissue compared with control levels at all ages examined (Fig. 1E).

Activation of the Rho/Rac/Cdc42 GTPases and Lim kinase in *Dhcr7*$^{\Delta 3\text{-}5/\Delta 3\text{-}5}$ brain tissue

Two homologous proteins, Lim kinase-1 and Lim kinase-2 (Limk), regulate cofilin activity by phosphorylation of serine 3. Limk-2 is ubiquitously expressed; however, Limk-1 expression is restricted to neuronal tissue. Both Limk-1 and Limk-2 are activated by threonine phosphorylation at amino acid position 505 and 508, respectively. Protein levels of Limk-1 and Limk-2 are similar in *Dhcr7*$^{+/+}$ or *Dhcr7*$^{\Delta 3\text{-}5/\Delta 3\text{-}5}$ embryonic brain tissue (Fig. 2A). However, consistent with increased phosphorylation of cofilin, we found increased levels of phosphorylated Limk in E18.5 brains from *Dhcr7*$^{\Delta 3\text{-}5/\Delta 3\text{-}5}$ embryos compared with tissue from *Dhcr7*$^{+/+}$ embryos (Fig. 2A). Quantification of results showed no significant differences in total Limk-1 ($P = 0.66$) or Limk-2 ($P = 0.74$) protein levels; however, P-Limk-1/2 levels were significantly ($P < 0.005$) increased in SLOS brain tissue (Fig. 2B). The antibody used to detect phosphorylation of Limk does not differentiate between Limk-1 and Limk-2. The ratio of P-Limk 1/2 relative to either Limk-1 ($P < 0.01$) or Limk-2 ($P < 0.05$) was significantly elevated in mutant brain tissue.

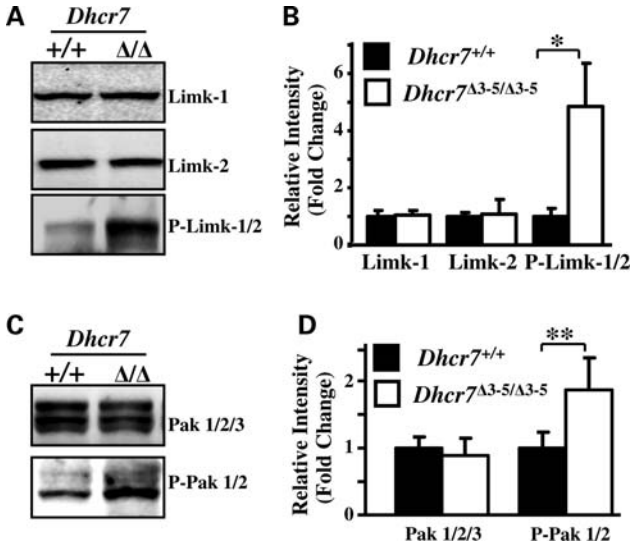

Figure 2. Limk and Pak activation. Western blot analysis (**A**) and quantification of band intensity (**B**) demonstrated similar amounts of immunoreactive Limk-1 and Limk-2 in *Dhcr7*$^{+/+}$ (filled bars) and *Dhcr7*$^{\Delta 3\text{-}5/\Delta 3\text{-}5}$ (open bars) E18.5 embryonic brain protein samples; however, phospho(Thr508)/Thr505)-Limk-1/2 levels were significantly increased (mean $\pm$ SD, $n = 5$, $^{*}P < 0.01$) in mutant brain tissue. The P-Limk antibody does not discriminate between Limk-1 and Limk-2. Western blot analysis (**C**) and quantification of band intensity (**D**) demonstrated similar amounts of immunoreactive Pak 1/2/3 in *Dhcr7*$^{+/+}$ and *Dhcr7*$^{\Delta 3\text{-}5/\Delta 3\text{-}5}$ E18.5 embryonic brain protein samples; however, P-Pak1/2 levels were significantly increased (mean $\pm$ SD, $n = 5$, $^{**}P < 0.05$) in mutant brain tissue. The anti-Pak antibody recognizes Pak1, Pak2 and Pak3 and the anti-phosphoPak antibody recognizes both P-Pak1 and P-Pak2. Staining intensities for both Limk and Pak were normalized to actin staining intensity.

Activation of Limk is mediated by Rho GTPases and their effector kinases (20). To understand further the etiology of increased P-cofilin-1 and P-Limk-1/2, we analyzed the activity state of the Rho-GTPase/Rho kinase, Rac-GTPase/p21 associated kinase and Cdc42/p21-activated kinase signaling cascades. Limk can be phosphorylated by p21 associated kinases (Pak), and Pak family members are activated when phosphorylated. Pak protein levels did not significantly differ ($P = 0.45$) in brain tissue from *Dhcr7*$^{+/+}$ or *Dhcr7*$^{\Delta 3\text{-}5/\Delta 3\text{-}5}$ embryos. However, we found a significant ($P < 0.05$) increase in the level of phosphorylated Pak in brain tissue from *Dhcr7*$^{\Delta 3\text{-}5/\Delta 3\text{-}5}$ embryos (Fig. 2C and D). Phosphorylation of Pak is mediated by Rac1 and Cdc42, which are small GTPases that cycle between an inactive state binding GDP and an active state binding GTP. Neither total levels of Rac1 (Fig. 3A and B) nor total levels of Cdc42 (Fig. 3C and D) immunoreactive material differed significantly ($P = 0.30$ and $P = 0.69$, respectively) between E18.5 brain tissue from *Dhcr7*$^{+/+}$ or *Dhcr7*$^{\Delta 3\text{-}5/\Delta 3\text{-}5}$ embryos. However, using Rac-GTP and Cdc42-GTP pull-down assays, we found that both activated Rac and Cdc42 levels were significantly increased ($P < 0.001$ and $P < 0.01$, respectively) in brain tissue from *Dhcr7*$^{\Delta 3\text{-}5/\Delta 3\text{-}5}$ embryos compared with control tissue (Fig. 3A–D). We were not able to directly demonstrate the activation of Rock;

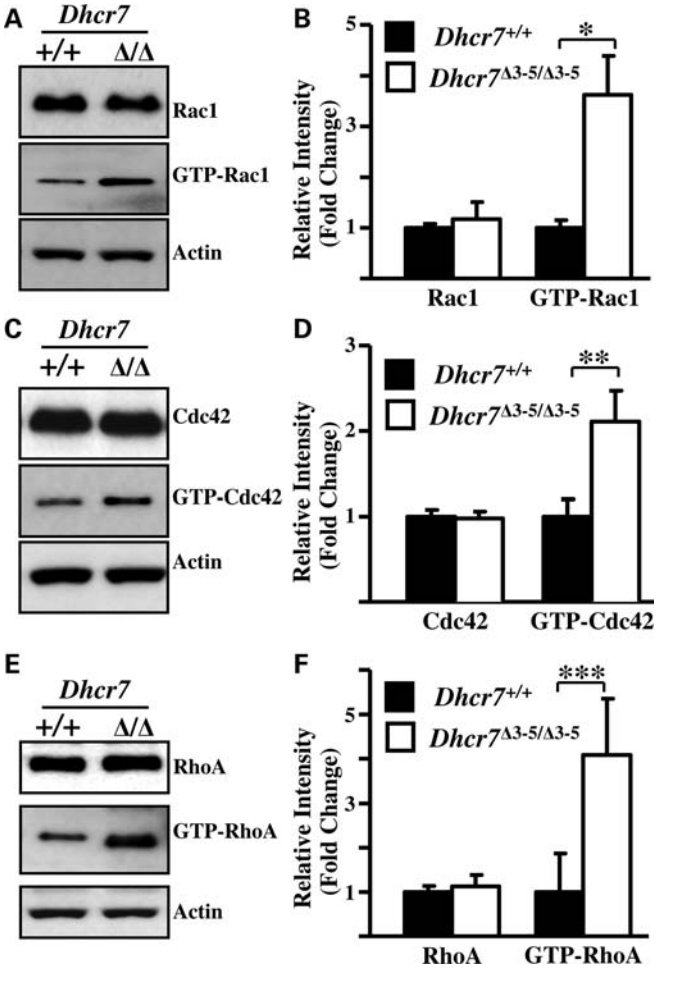

Figure 3. Rho GTPase activation. Although total protein levels were not altered, the levels of GTP activated Rac1 (**A** and **B**), Cdc42 (**C** and **D**) and RhoA (**E** and **F**) were significantly increased (mean ± SD; $n = 5$; $^{*}P < 0.001$, $^{**}P < 0.01$, $^{***}P < 0.05$) in *Dhcr7* mutant tissue (open bars) compared with control samples (filled bars). Band intensity was normalized to actin.

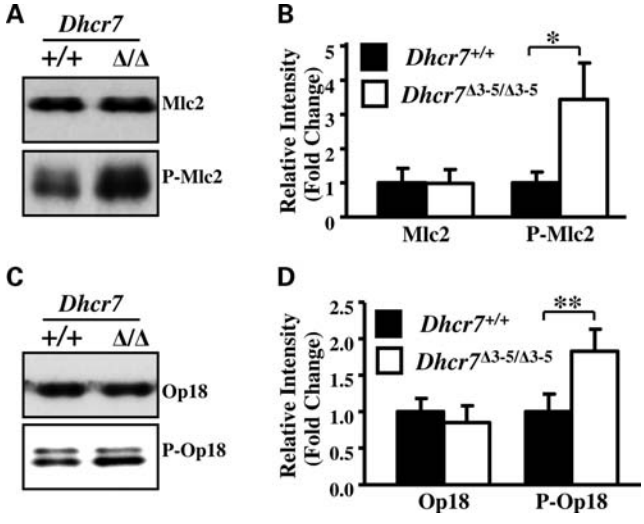

Figure 4. Increased phosphorylation of Mlc2 and OP18. Western blot analysis (**A** and **C**) and quantification of band intensity (**B** and **D**) demonstrated similar amounts of immunoreactive Mlc2 or Op18 in $Dhcr7^{+/+}$ (filled bars) and $Dhcr7^{\Delta 3\text{-}5/\Delta 3\text{-}5}$ (open bars) mouse brain protein samples. In contrast, phospho(Ser19)-Mlc2 and phospho(Ser16)-Op18 levels were significantly increased in $Dhcr7^{\Delta 3\text{-}5/\Delta 3\text{-}5}$ brain tissue (mean ± SD; $n = 5$; $^{*}P < 0.01$ and $^{**}P < 0.05$). Band intensity was normalized to actin (data not shown).

however, we were able to use Rho-GTP pull-down assays to demonstrate significantly ($P < 0.05$) increased activation of RhoA (Fig. 3E and F). Similar to what was observed for Rac1 and Cdc42, no significant difference ($P = 0.64$) in immunoreactive RhoA was observed (Fig. 3E and F). The activation of RhoA, Rac1 and Cdc42 appears to be specific and not due to non-specific activation of small GTPases. A Ras-GTP pull-down assay was used to evaluate the activation status of Ras in *Dhcr7* mutant and control embryonic brain tissue. In contrast to what we observed with RhoA, Rac1 and Cdc42, we did not observe increased activation of Ras (Supplementary Material, Fig. S2). Supporting the idea that the activation of the Rho GTPase/LIM kinase regulatory cascade is not due to a non-specific mechanism, we did not observe increased phosphorylation of protein kinase A Cα, a protein that is regulated by G protein-coupled receptors (Supplementary Material, Fig. S3).

In addition to cofilin-1, the Rho/Rac/Cdc42 signaling cascades regulate other cytoskeletal proteins (23). Rock phosphorylates myosin light chain 2 (Mlc2) and regulates myosin/actin interactions. Mlc2 functions in both early and late stages of neuronal morphogenesis (24,25). Consistent with the increased activation of RhoA, analysis of Mlc2 expression showed similar Mlc2 protein levels in $Dhcr7^{+/+}$ and $Dhcr7^{\Delta 3\text{-}5/\Delta 3\text{-}5}$ E18.5 brain tissue, but significantly increased (3.4-fold, $P < 0.005$) levels of phosphorylated Mlc2 in $Dhcr7^{\Delta 3\text{-}5/\Delta 3\text{-}5}$ tissue (Fig. 4A and B). Pak phosphorylates and inactivates Op18 (Stathmin), and Op18 regulates microtubule assembly (26). Although Op18 protein levels did not differ between control and *Dhcr7* mutant embryos, consistent with increased Pak activity, we observed increased phosphorylation (1.8-fold, $P < 0.015$) of Op18 in brain tissue from E18.5 $Dhcr7^{\Delta 3\text{-}5/\Delta 3\text{-}5}$ embryos (Fig. 4C and D).

Altered cofilin phosphorylation is due to cholesterol deficiency

In $Dhcr7^{\Delta 3\text{-}5/\Delta 3\text{-}5}$ brain tissue, there is both a deficiency of cholesterol and accumulation of 7DHC (12). Thus, observed abnormalities could result from sterol deficiency or a toxic effect of 7DHC. To separate these two potential mechanisms, we analyzed protein expression in brain tissue from $Sc5d^{+/+}$ control and $Sc5d^{-/-}$ mutant embryos. Sc5d, or lathosterol 5-desaturase, catalyzes the enzymatic step immediately upstream of Dhcr7 and converts lathosterol to 7DHC (Fig. 1A). In $Sc5d^{-/-}$ embryos, there is a cholesterol deficiency similar to that observed in $Dhcr7^{\Delta 3\text{-}5/\Delta 3\text{-}5}$ brains, but lathosterol, rather than 7DHC, is the accumulating sterol (27). Altered cofilin-1 expression was identified in a 2-DE proteomic comparison of brain tissue from E18.5 $Sc5d^{+/+}$ and $Sc5d^{-/-}$ embryos (Fig. 5A and B). Analogous to what was observed in the SLOS mouse model, cofilin-1 protein levels were constant, but cofilin-1 phosphorylation was increased in embryonic brain tissue from the lathosterolosis mouse

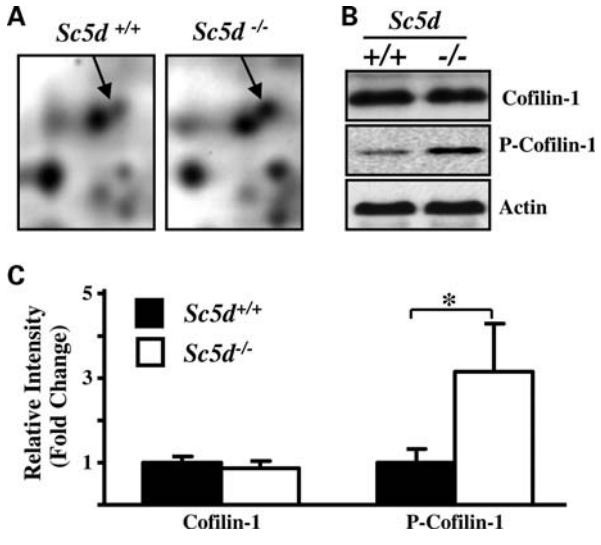

Figure 5. Increased phosphorylation of Cofilin in $Sc5d^{-/-}$ mouse brains. (**A**) Representative portions of 2-DE gels comparing proteins from E18.5 $Sc5d^{+/+}$ and $Sc5d^{-/-}$ E18.5 brain tissue. The differentially expressed spot identified by the arrows was later shown by mass spectrometric analysis to contain cofilin-1. (**B**) Although total cofilin-1 levels did not differ, increased expression of P-cofilin-1 in *Sc5d* mutant brain tissue was validated by western blot. (**C**) Quantification of cofilin-1 and P-cofilin-1 protein levels confirmed a significant increase in P-cofilin 1 expression (mean $\pm$ SD; $n = 5$; $^*P < 0.01$) Band intensity was normalized to that of actin.

model (Fig. 5B and C). In addition, consistent with our findings in the *Dhcr7* mutant brain tissue, Limk-1/2, Pak, Op18 and Mlc2 phosphorylation were all significantly increased in *Sc5d* mutant brain tissue (Supplementary Material, Fig. S4). The similar proteomic phenotype in $Sc5d^{-/-}$ and $Dhcr7^{\Delta 3\text{-}5/\Delta 3\text{-}5}$ embryonic brain tissue strongly argues that this specific defect is due to a deficiency of cholesterol rather than a toxic effect of the accumulating intermediate.

In vivo disruption of actin filaments in embryonic $Dhcr7^{\Delta 3\text{-}5/\Delta 3\text{-}5}$ brain tissue

Cofilin-1 regulates actin filament formation by severing F-actin filaments and increasing barbed ends that can function as *de novo* filament nucleation sites. Thus increased phosphorylation of cofilin-1, as shown above, would be predicted to alter actin filament formation *in vivo*. To evaluate *in vivo* actin filament formation, we stained embryonic brain sections with rhodamine labeled phalloidin. Phalloidin is a toxin that binds to filamentous actin (F-actin). Thus, increased rhodamine-phalloidin staining is consistent with decreased cofilin-1 activity. Rhodamine-phalloidin stained midsagital brain sections from E18.5 $Dhcr7^{+/+}$ and $Dhcr7^{\Delta 3\text{-}5/\Delta 3\text{-}5}$ embryos are shown in Figure 6A and B. Quantification of fluorescence intensity in nine anatomical domains determined from analysis of nine midsagital sections from three control and three *Dhcr7* mutant embryos showed that total phalloidin staining was increased an average of 1.26-fold ($P = 0.005$) in brains from $Dhcr7^{\Delta 3\text{-}5/\Delta 3\text{-}53\text{-}5}$ embryos compared with controls. We noted regional difference in phalloidin staining, thus we analyzed staining intensity separately for each of the nine anatomical domains (Fig. 6C). After correction for multiple comparisons, we found significantly increased phalloidin staining in the caudate-putamen (1.44-fold, $P < 0.05$), optic area (1.73-fold, $P < 0.001$) and the fimbria (1.91-fold, $P < 0.01$). Although not significant after accounting for multiple comparisons, we noted trends toward increased staining in hippocampus and geniculate area and decreased staining in the cortical plate.

In vitro analysis of dendrite and axonal growth

Rho and Rac/Cdc42 differentially regulate dendritic and axonal growth in the developing central nervous system. Thus, we hypothesized that a perturbation of Rho/Rac/Cdc42 activity would functionally be reflected in dendritic number, dendritic length or axonal length. To test this, we prepared hippocampal neurons from E18.5 $Dhcr7^{+/+}$ and $Dhcr7^{\Delta 3\text{-}5/\Delta 3\text{-}5}$ and maintained neurons in cholesterol deficient medium. Biochemically, these neurons have markedly reduced cholesterol and increased 7DHC levels (Supplementary Material, Table S1). At 7 days *in vitro* (DIV7), neurons were transfected with a construct expressing green fluorescent protein. Three days after transfection, neurons were fixed and confocal images were obtained. Although no significant difference in the number of dendrites was present, we observed an increase in the total length of both dendrites and axons in neurons derived from $Dhcr7^{\Delta 3\text{-}5/\Delta 3\text{-}5}$ embryos compared with neurons derived from $Dhcr7^{+/+}$ embryos (dendrite: increased by 1.47-fold, $P = 0.02$; axon: increased by 1.53-fold, $P = 0.004$; Figure 6D and E).

DISCUSSION

SLOS is an inborn error of cholesterol synthesis with a pleiotropic phenotype. In addition to variable congenital anomalies, patients with SLOS have variable degrees of mental retardation and a distinct behavioral phenotype (28). One of the more intriguing aspects of the behavior phenotype is that the majority of patients have autistic traits and more than half of the patients meet the diagnostic criteria for autism (28,29). Although the biochemical defect in SLOS is well described, the pathophysiological consequences of decreased cholesterol or increased 7DHC that underlie the learning and behavioral problems found in SLOS are not well defined. Defining these pathological processes and determining to what extent they are due to fixed developmental problems or due to functional defects secondary to the altered sterol composition in the brain is critical to determining if therapeutic interventions could impact the neurological deficits.

In order to try to address these questions, mouse models of SLOS have been produced (12,15,16). $Dhcr7^{\Delta 3\text{-}5/\Delta 3\text{-}5}$ pups replicate the biochemical defect found in severely affected SLOS infants, have significant neurological problems, and die soon after birth secondary to abnormal suckling and failure to feed (12). We thus hypothesized that a proteomic comparison of tissue isolated from $Dhcr7^{+/+}$ and $Dhcr7^{\Delta 3\text{-}5/\Delta 3\text{-}5}$ embryos would provide an unbiased technique to identify novel biological pathways whose normal function could be impaired in SLOS. One of the proteins that we identified in this analysis was cofilin-1. Recognition of altered cofilin-1 phosphorylation

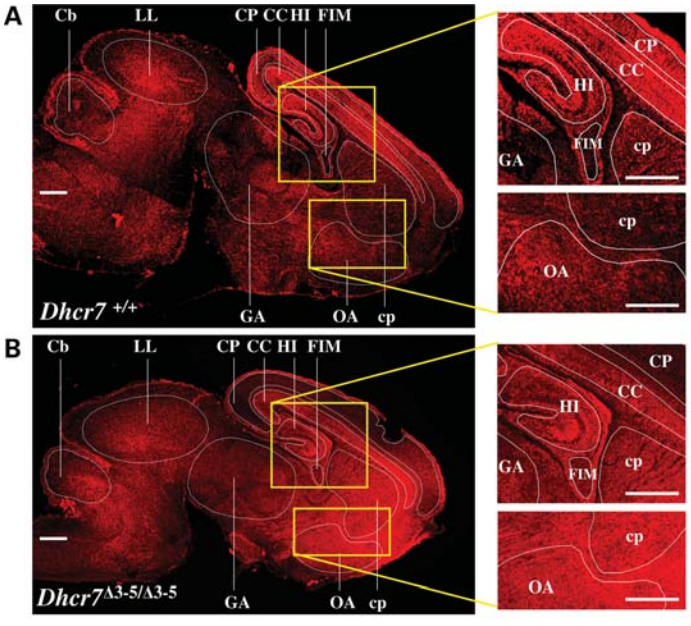

C

Structure	Intensity Ratio Δ/Δ :+/+	p -value
CP	0.76	NS
CC	1.06	NS
HI	1.25	NS
FIM	1.91	p<0.001
cp	1.44	p<0.05
OA	1.73	p<0.001
GA	1.33	NS
LL	1.02	NS
Ch	1.37	NS

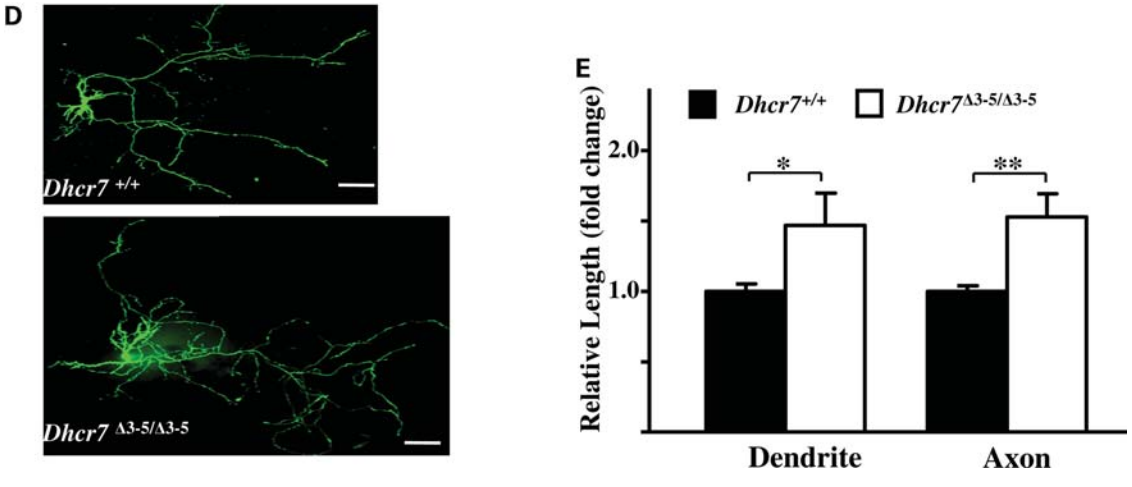

Figure 6. *In vivo* disruption of actin polymerization and, *in vitro* analysis of dendrite and axonal growth. Sagittal sections of E18.5 *Dhcr7* control (**A**) and mutant (**B**) brain tissue were stained with rhodamine labeled phalloidin to detect endogenous levels of filamentous actin. Fluorescent intensity was quantified for nine tissue sections from three embryos corresponding to each genotype. When compared with controls, overall staining intensity was increased 1.26-fold in sections from $Dhcr7^{\Delta 3\text{-}5/\Delta 3\text{-}5}$ embryos ($P = 0.005$). (**C**) Fluorescent intensity was also measured in nine anatomical subdivisions (CP: cortical plate; CC: corpus callosum; HI: hippocampus; FIM: fimbria; cp, caudate-putamen; OA: optic area; LL: lateral lemniscus; Cb: cerebellum; GA: geniculate). After correction for multiple comparisons, $Dhcr7^{\Delta 3\text{-}5/\Delta 3\text{-}5}$:$Dhcr7^{+/+}$ intensity ratio was found to be significantly increased in the caudate-putamen, optic area and fimbria. Scale bar indicates 500 μm. (**D**) Hippocampal neurons from E18.5 *Dhcr7* control and mutant embryos were transfected with a green fluorescent protein expression vector to visualize axons and dendrites, and grown for 10 days in cholesterol-free medium. Representative images of $Dhcr7^{+/+}$ and $Dhcr7^{\Delta 3\text{-}5/\Delta 3\text{-}5}$ neurons. Both axonal and dendritic length were increased in $Dhcr7^{\Delta 3\text{-}5/\Delta 3\text{-}5}$ neurons. Scale bar indicates 100 μm. (**E**) Axon and dendrite length were measured for 21 *Dhcr7* control (filled bar) and 14 *Dhcr7* mutant (open bar) neurons. Relative axonal and dendritic length are shown (mean ± SEM; $^{*}P < 0.05$ and $^{**}P < 0.01$).

in *Dhcr7* mutant embryonic brain tissue subsequently provided novel insight into a disturbance of axonal and dendrite growth that may underlie some of the learning and behavioral problems found in SLOS patients.

Cofilin-1 is an actin depolymerization factor that plays a central role in the regulation of the neuronal actin cytoskeleton (19). Active cofilin-1 functions to sever actin filaments and increase actin turnover. As such, cofilin-1 plays a major role in axonal and dendritic growth. The activity of cofilin-1 is regulated by phosphorylation. Phosphorylation of cofilin-1 on serine-3 by Lim kinase inactivates cofilin-1 and promotes actin filament formation (20,30). Lim kinase is activated by phosphorylation which is mediated by both Rho-kinase (Rock) and p21-activated kinase (Pak). Rock and Pak are serine/threonine protein kinases that are regulated by the Rho family of GTPases (31,32). The Rho family of GTPases functions as molecular switches that are activated by the binding of GTP. Active Rac1 and active Cdc42, in general, promote axonal and dendritic elongation; whereas active RhoA in general antagonizes axonal and dendritic growth.

However, both Rock and Pak regulate Lim kinase in a similar manner, thus a balance of activity between the two pathways is critical for the dynamic regulation of axon and dendrite growth (31). Our proteomic screen identified cofilin-1 in one of the protein spots showing differential expression in brain tissue from *Dhcr7* mutant embryos. Validation of this result showed that although cofilin-1 protein levels were similar in control and mutant tissue, levels of P-cofilin-1 were significantly increased in brain tissue from $Dhcr7^{\Delta 3\text{-}5/\Delta 3\text{-}5}$ embryos. We then characterized the activation state of multiple steps in this regulatory cascade. Consistent with increased cofilin-1 phosphorylation, we found increased phosphorylation of both Limk and Pak, and increased activation of RhoA, Cdc42 and Rac1.

As noted above, RhoA, Rac1 and Cdc42 act to regulate axon and dendritic growth by modulating actin cytoskeleton. We thus postulated that altered RhoA, Rac1 and Cdc42 activity in *Dhcr7* mutant embryonic brain tissue would have functional consequences. Rhodamine-phalloidin staining of embryonic brain tissue demonstrated increased levels of filamentous actin in $Dhcr7^{\Delta 3\text{-}5/\Delta 3\text{-}5}$ brain tissue compared with $Dhcr7^{+/+}$ tissue. The neonatal death of $Dhcr7^{\Delta 3\text{-}5/\Delta 3\text{-}5}$ mice precludes a direct *in vivo* demonstration of altered axon and dendrite length in SLOS brain tissue. Thus, we studied axon and dendrite growth *in vitro*. Again, consistent with altered function of the Rho/Rac/Cdc42 regulatory cascade in *Dhcr7* mutant brain tissue, we found that both axon and dendrite length were significantly increased in hippocampal neurons derived from *Dhcr7* mutant embryos.

Increased phosphorylation of cofilin-1, Limk-1/2, Pak, Op18 and Mlc2 was observed in brain tissue from both $Dhcr7^{\Delta 3\text{-}5/\Delta 3\text{-}5}$ and $Sc5d^{-/-}$ embryos. As SLOS and lathosterolosis mouse models have similar cholesterol deficiencies but different accumulating precursor sterols, we postulate that the cholesterol deficiency in SLOS, rather than the accumulation of 7DHC, underlies altered activation of Rho GTPases that regulate axonal and dendritic growth. This aberrant activation unbalances the dynamic regulation that RhoA and Rac/Cdc42 exert on axon and dendritic growth.

Various hypotheses could explain increased activation of Rho GTPases in SLOS. Posttranslational prenylation of Rho GTPases results in the adduction of a geranylgeranyl moiety, and prenylation of Rho GTPases is required for membrane association and function. Rho GTPases become membrane associated and activated when post-translationally modified by prenylation. Thus, it is plausible that increased prenylation due to increased production of geranylgeranyl in mutant tissue could lead to increased activation of Rho GTPases. A number of observations are consistent with this hypothesis. First, this proteomic analysis of $Dhcr7^{\Delta 3\text{-}5/\Delta 3\text{-}5}$ and $Sc5d^{-/-}$ embryos also identified increased expression of hydroxymethylglutaryl-CoA synthase and isopentenyl-diphosphate delta-isomerase 1 (unpublished data). These two cholesterol synthetic enzymes are also involved in the synthesis of geranylgeranyl. Second, Pappu *et al*. (33) have shown increased synthesis of other nonsterol isoprenoid-derived compounds in SLOS. It is plausible that the inhibition of Rho GTPase prenylation in SLOS could be a novel therapeutic intervention. Inhibition of protein prenylation has been developed as anticancer therapies (34) and protein prenylation inhibitors may be useful in the treatment of Hutchinson-Gilford Progeria (35,36). An alterative hypothesis is that altered sterol composition in the plasma membrane alters the function of membrane proteins which regulate Rho GTPase function. Rho GTPases integrate extracellular signals via the combined action of multiple GTPase-activating proteins (GAPs) and guanine nucleotide exchange factors (GEFs) that respond to various extracellular signals. Semiphorins and ephrins are membrane associated signaling proteins that regulate axon growth and guidance via effects on Rho GTPase activity, and alteration of cholesterol-rich lipid microdomains may affect the function of semiphorins (37) and ephrins (38). Biophysical properties and functions of cholesterol-rich microdomains are altered in SLOS (8–10). NMDA receptor function has also been shown to regulate Rho GTPase function (39), and our previous characterization of the *Dhcr7* mutant mouse demonstrated impaired NMDA glutamate receptor activity (12). Independent of the specific mechanism that results in altered Rho GTPase function in SLOS, it is plausible that this abnormality underlies some of the cognitive defects found in SLOS. Altered Rho GTPase function has been implicated in a number of syndromic and non-syndromic genetic disorders with cognitive impairment (21,31). X-linked mental retardation has been associated with mutations of (i) *OPHN1*, a GAP for Rho GTPases (40,41); (ii) α*PIX/ARHGEF6*, a Rac GEF (42); (iii) *FGD1*, an activator of CDC42 (43,44); and (iv) *PAK3* (45). Williams syndrome is a chromosome 7q11.2 contiguous gene deletion syndrome that includes *LIMK1* (46). Although deletion of other genes may contribute to the cognitive phenotype observed in Williams syndrome, Limk-1 deficient mice have abnormal dendritic spine morphology and altered spatial learning (47). Although appropriately fixed human SLOS brain tissue is not currently available to directly confirm the presence of axonal and dendritic abnormalities, based on the association of defects in Rho GTPase signaling with mental retardation syndromes (23) and the data presented in this paper, it is likely that altered axon and dendrite formation underlies some of the central nervous system dysfunction found in SLOS. Future efforts will focus on determining if inhibition of protein prenylation or if modulation of specific signal transduction pathways related to axon and dendrite growth is of potential therapeutic benefit in SLOS.

MATERIALS AND METHODS

Mouse models

Animal work was performed under an NICHD approved animal study protocol. *Dhcr7* and *Sc5d* mutant mouse models and genotyping have previously been described (12,27). For timed matings, the identification of a copulatory plug was considered to be E0.5 and embryonic age was confirmed by inspection.

Protein sample preparation

Mouse brain tissue samples were rapidly dissected from E18.5 embryos and immediately washed with ice-cold 1 × phosphate buffered saline (PBS). Tissue samples were then homogenized

in 500 μl of lysis buffer [7 M urea, 2 M Thiourea, 4% CHAPS, 65 mM DTT, 40 mM Tris, protease inhibitor mix and phosphoprotease inhibitor (0.2 mM Na_3VO_4, 1 mM NaF)]. After homogenization, the sample was sonicated at 100 W for 30 s and centrifuged at 25 000*g* for 1 h. Protein samples from 7 or 8 individual embryos corresponding to each genotype (*Dhcr7*$^{+/+}$, *Dhcr7*$^{\Delta 3\text{-}5/\Delta 3\text{-}5}$, *Sc5d*$^{+/+}$ and *Sc5d*$^{-/-}$) were pooled. Pooled samples were used for 2-DE analysis and initial validation. For the temporal expression experiment, protein samples from 4 or 5 individual control or *Dhcr7*$^{\Delta 3\text{-}5/\Delta 3\text{-}5}$ embryos at E12.5, E14.5 and E16.5 were pooled. Protein concentration was determined using a Bradford assay. Samples were stored at −80°C until analysis.

Two-dimensional protein gel electrophoresis and identification of differentially expressed protein spots

Immobilized pH Gradient Isoelectric focusing (IPG-IEF) was performed using an Ettan IPGphor 3 IEF System (GE Healthcare). Each genotype was analyzed in triplicate. Eighty micrograms of protein were mixed with DeStreak™ Rehydration Solution (GE Healthcare) containing 1% IPG-IEF buffer, pH 3–10 non-linear, 0.2% DTT and a trace of bromophenol blue to give a total volume of 250 μl. This solution was then loaded onto precast IPG dry strips (pH 3–10; 130 mm × 3 mm × 0.5 mm; GE Healthcare) and rehydrated at 30 V for 12 h. IEF was performed at 20°C using stepped voltage changes of 500 V for 1 h, 1000 V for 1 h and 8000 V for 8 h for a total of 50–60 kV h.

Following IEF separation, the gel strips were equilibrated twice (15 min each) in an equilibration buffer composed of 50 mM Tris–HCl pH 8.8, 6 M urea, 30% glycerol, 2% SDS and a trace of bromophenol blue. One percent DTT was added to the first equilibration buffer, and 4.5% iodoacetamide was added to the second equilibration buffer. The equilibrated gel strips were then placed onto 1 mm 12% polyacrylamide vertical slab gels, and sealed with 0.5% agarose. SDS–PAGE was performed using a Hoeffer SE600 Ruby Electrophoresis Unit (GE Healthcare) for 15 min at constant current of 10 mA per gel, and then switched to 20 mA per gel until the Bromophenol blue reached the bottom of the gels.

After two-dimensional gel electrophoretic separation, gels were stained with ammoniacal silver nitrate (48). Stained gels were scanned at an optical resolution of 42.3 × 42.3 μm using a GS-800 Calibrated Densitometer (Bio-Rad) in transmissive mode. Spot detection, matching, quantization, normalization and statistical analysis for the triplicate silver-stained analysis gels for mouse brain samples of different genotype were performed using PDQuest 8.0 software (Bio-Rad) as previously described (48). The PDQuest software models protein spots mathematically as a 3D Gaussian distribution and determines maximum absorption after raw image correction and background subtraction. Spot intensities were then obtained by the integration of the Gaussian function with unit of intensity calculated as 'Intensity*Area as parts per million' (INT*Area PPM). The intensity of each protein spot was normalized to the total intensity of the entire gel. Quantitative analysis was performed using the Student's *t*-test between control and *Dhcr7*$^{\Delta 3\text{-}5/\Delta 3\text{-}5}$ or *Sc5d*$^{-/-}$ mutant mouse brain gels. The confidence level was 95% ($P < 0.05$).

After identification of candidate protein spots, preparative 2-DE was performed with 2 mg of protein loaded on each gel. Protein spots were identified using Coomassie Brilliant Blue R-250 Staining Solutions (Bio-Rad) per manufacturer's protocol. Protein spots were excised from paired control and mutant preparative gels for protein identification.

Mass spectrometric protein identification

Excised protein spots were 'in-gel' digested with trypsin, and resulting peptides were extracted. Peptides were analyzed both by MALDI TOF/TOF using an ABI 4800 Proteomics Analyzer (Applied Biosystems) and by combined liquid chromatography/tandem mass spectrometry (LC/ESI/MS/MS) using an LCQ DECA ion trap mass spectrometer (Thermo Fischer).

For MALDI TOF/TOF analysis, tryptic peptides were applied as unseparated mixtures to sample plate wells. Typically 0.5 μl of extracted peptide, 5% of total sample in 1:1 acetonitrile: 0.1% TFA was applied with an equal volume of HCCA matrix (5 mg/ml in the same solvent as the sample); two internal standards were added to the matrix and along with tryptic autolysis peptides were used for mass scale calibration. Our typical procedure was to acquired a 400 laser shot spectrum of the full peptide mixture in reflector mode and then to fragment 4–6 peptides that are both intense and well separated from others within the limits of the timed ion selector operated at a resolution of 300; fragmentation spectra were acquired as unimolecular decompositions (collision gas off) using 1000 laser shots. There is no evidence of sample depletion from this approach.

For the LC/ESI/MS/MS measurements, tryptic peptides were separated by reversed phase chromatography and electrosprayed directly into the sampling orifice of the mass spectrometer. MS/MS spectra were collected in a data-dependent manner, with up to three of the most intense ions in each full MS scan being subjected to isolation and fragmentation. MS/MS spectra were extracted as dta files using default parameters with BioWorks v2.0 (Thermo Fisher). For each LC/MS/MS, run the dta files were merged into one database file prior to analysis.

MS/MS spectra from both the MALDI and LC/ESI measurements were analyzed to identify specific proteins. The Mascot v 2.2 (Matrix Science) search program was used to match both b and y ion series to protein sequences present in the *Mus musculus* subset of UniProt KB/Swiss-Prot/TrEMBL database (database version 56.0; 392 667 sequence entries, 22 July 2008). Mascot search parameters were as follows: enzyme, trypsin; one missed tryptic cleavage site permitted; fixed modification, carbamidomethylation of cysteine; variable modification, methionine oxidation; mass tolerance for precursor ions was ±1.2 Da (DECA) and ±0.15 Da (4800); mass tolerance for fragment ions, ±0.6 Da (DECA) and ±0.06 Da (4800). Only peptides with individual ions Mowse scores >32 indicating significant identity or extensive homology ($P < 0.05$) were used for protein identification. Peptide and protein identifications were validated using Scaffold v2.2 (Proteome Software, Portland, OR, USA). In Scaffold, the peptide identifications from Mascot were verified using the X! Tandem

(www.thegpm.org v 2007.01.0.2) database search program (49). Probabilistic validations of the peptide identifications were performed using Peptide Prophet (50) and corresponding protein probabilities by Protein Prophet (51). The cutoff for peptide identification was set at greater than 95.0% probability and protein identification at greater than 99% probability with two or more identified peptides.

Western blot analysis

Twenty micrograms of protein were separated on 4–12% Nupage Tris-acetate gels (Invitrogen) and transferred to a nitrocellulose membrane using iBlot (Invitrogen) according to the manufacture's protocol. Chemiluminescent western blotting was performed using the Western Breeze kit from Invitrogen per manufacture's protocol. The following primary antibodies were used for western blot analysis: mouse monoclonal anti-actin (1:5000; Sigma), anti-cofilin-1 (1:2000; Cell Signaling Technology), anti-phospho-Cofilin (Ser3) (1:200; Cell Signaling Technology), rabbit polyclonal anti-Limk-1 (1:1000; Cell Signaling Technology), rabbit polyclonal anti-Limk-2 (1:1000; Cell Signaling Technology), rabbit polyclonal anti-phospho-Limk1 (Thr508)/Limk-2 (Thr505) (1:200; Cell Signaling Technology), rabbit polyclonal anti-Pak1/2/3 (1:1000; Cell Signaling Technology), rabbit polyclonal anti-phospho-Pak1 (Thr423)/Pak2 (Thr402) (1:200; Cell Signaling Technology), rabbit polyclonal anti-Mlc2 (1:1000; Cell Signaling Technology), rabbit polyclonal anti-phospho-Mlc2 (Ser19) (1:200; Cell Signaling Technology), mouse monoclonal anti-OP18 (1:2000; Santa Cruz Biotechnology), rabbit polyclonal anti-phospho-Op18 (Ser 16) (1:400; Santa Cruz Biotechnology). Band intensity on western blots was quantified and normalized to intensity obtained for actin. For quantitative analysis, five individual samples were analyzed. Data are expressed as the mean and standard deviation.

GTPase activation assay

RhoA, Rac1, Cdc42 and Ras activation assays were performed by using small GTPase activation assay kits (Cytoskeleton, Denver, CO, USA) per manufacture's protocol. Briefly, brains were isolated from five E18.5 embryos for each genotype and were lysed using the provided buffer. Total RhoA, Rac1 and Cdc42 levels were determined by western blot analysis of 20 mcg of total protein. For the determination of activation status, 300 mcg of the protein lysate was incubated with either RBD or PBD glutathione beads for 1 h at 4°C. After washing, the bound proteins were analyzed by western blotting with monoclonal antibody against RhoA, Rac1, Cdc42 or Ras to detect GTP-RhoA, GTP-Rac1 and GTP-Cdc42, respectively.

Histological analysis

For phalloidin staining heads from E18.5 *Dhcr7* control and mutant embryos were fixed overnight at 4°C in PBS (pH 7.4) with 4% paraformaldehyde. After washing in PBS, the tissues were equilibrated in 30% sucrose/PBS (pH 7.4). Sagittal sections were cut at a thickness of 20 μm on a Leica Cryostat, model CM-3050S. Cryostat sections were washed for 30 min with 50 mM glycine-PBS containing 0.5% coldwater fish gelatin to block non-specific binding, and then incubated for 2 h in a PBS solution containing 1.5 U rhodamine phalloidin (Invitrogen), 0.5% cold water fish gelatin and 50 mM glycine. For a negative control, the rhodamine phalloidin was omitted. After washing in PBS, the stained sections were mounted using MOWIOL media. Fluorescent microscopy was performed on a Zeiss LSM 510 inverted microscope using 5× (NA 0.15) objective lens. With the same laser intensity, the fluorescent images for $Dhcr7^{+/+}$ and $Dhcr7^{-/-}$ mouse brains were obtained. The fluorescent intensity was analyzed with MetaMorph software (Universal Imaging). Nine sections were analyzed from each brain and three brains were analyzed for each genotype. Whole brain section fluorescent intensity was compared using a two-tailed Student *t*-test. To account for multiple comparisons, fluorescent staining for specific anatomical regions was analyzed using one-way analysis of variance (ANOVA) with Bonferroni correction for multiple comparisons.

Hippocampal dendrite and axonal length analysis

Hippocampal neuron cultures were prepared and immunostained as previously described (52). Briefly, the hippocampus was dissected from $Dhcr7^{+/+}$ and $Dhcr7^{\Delta 3\text{-}5/\Delta 3\text{-}5}$ E18.5 embryos, digested with 0.125% trypsin, seeded onto poly-D-lysine (Sigma)-coated coverslips at a density of 2×10^5 cells/cm^2, and cultured in Neurobasal medium (Invitrogen) supplemented with B27 (Invitrogen). Cells were grown at 37°C in a humidified atmosphere of 5% CO_2. The B27/Neurobasal medium has no detectable cholesterol by gas chromatographic/mass spectrometric analysis (data not shown). Neurons were transfected at DIV7 with a plasmid expressing Venus with Lipofectamine 2000 (Invitrogen) per manufacture's instructions. Three days after transfection, neurons were fixed in PBS containing 4% paraformaldehyde for 15 min at room temperature. Fixed neurons were stained with a rabbit anti-GFP antibody (MLB) and an Alexa 488-conjugated secondary antibody (Invitrogen). Images were acquired using an inverted Zeiss LSM510 confocal microscope with a 10× (NA 0.25) objective. Dendrites and axons from collapsed confocal images were manually traced and measured with MetaMorph software (Universal Imaging).

SUPPLEMENTARY MATERIAL

Supplementary Material is available at *HMG* online.

ACKNOWLEDGEMENTS

The authors would like to thank Macelo Diaz Butamante, Kirstyn Brownson, Meghan Lyman and Erin Merkel for their assistance.

Conflict of Interest statement. None declared.

FUNDING

This work was supported by the intramural research program of the *Eunice Kennedy Shriver* National Institute of Child Health, National Institutes of Health; and the intramural research program of the National Institute of Mental Health, National Institutes of Health. Microscopy imaging was performed at the Microscopy & Imaging Core (National Institute of Child Health and Human Development, NIH) with the assistance of Dr Vincent Schram, Chip Dye and Dr James T. Russell.

REFERENCES

1. Porter, F.D. (2008) Smith–Lemli–Opitz syndrome: pathogenesis, diagnosis and management. *Eur. J. Hum. Genet.*, **16**, 535–541.
2. Fitzky, B.U., Witsch-Baumgartner, M., Erdel, M., Lee, J.N., Paik, Y.K., Glossmann, H., Utermann, G. and Moebius, F.F. (1998) Mutations in the Delta7-sterol reductase gene in patients with the Smith–Lemli–Opitz syndrome. *Proc. Natl Acad. Sci. USA*, **95**, 8181–8186.
3. Wassif, C.A., Maslen, C., Kachilele-Linjewile, S., Lin, D., Linck, L.M., Connor, W.E., Steiner, R.D. and Porter, F.D. (1998) Mutations in the human sterol delta7-reductase gene at 11q12–13 cause Smith–Lemli–Opitz syndrome. *Am. J. Hum. Genet.*, **63**, 55–62.
4. Waterham, H.R., Wijburg, F.A., Hennekam, R.C., Vreken, P., Poll-The, B.T., Dorland, L., Duran, M., Jira, P.E., Smeitink, J.A., Wevers, R.A. *et al.* (1998) Smith–Lemli–Opitz syndrome is caused by mutations in the 7-dehydrocholesterol reductase gene. *Am. J. Hum. Genet.*, **63**, 329–338.
5. Correa-Cerro, L.S. and Porter, F.D. (2005) 3beta-hydroxysterol Delta7-reductase and the Smith–Lemli–Opitz syndrome. *Mol. Genet. Metab.*, **84**, 112–126.
6. Yu, H. and Patel, S.B. (2005) Recent insights into the Smith–Lemli–Opitz syndrome. *Clin. Genet.*, **68**, 383–391.
7. Tulenko, T.N., Boeze-Battaglia, K., Mason, R.P., Tint, G.S., Steiner, R.D., Connor, W.E. and Labelle, E.F. (2006) A membrane defect in the pathogenesis of the Smith–Lemli–Opitz syndrome. *J. Lipid Res.*, **47**, 134–143.
8. Gondre-Lewis, M.C., Petrache, H.I., Wassif, C.A., Harries, D., Parsegian, A., Porter, F.D. and Loh, Y.P. (2006) Abnormal sterols in cholesterol-deficiency diseases cause secretory granule malformation and decreased membrane curvature. *J. Cell Sci.*, **119**, 1876–1885.
9. Megha, Bakht, O. and London, E. (2006) Cholesterol precursors stabilize ordinary and ceramide-rich ordered lipid domains (lipid rafts) to different degrees. Implications for the Bloch hypothesis and sterol biosynthesis disorders. *J. Biol. Chem.*, **281**, 21903–21913.
10. Keller, R.K., Arnold, T.P. and Fliesler, S.J. (2004) Formation of 7-dehydrocholesterol-containing membrane rafts *in vitro* and *in vivo*, with relevance to the Smith–Lemli–Opitz syndrome. *J. Lipid Res.*, **45**, 347–355.
11. Kovarova, M., Wassif, C.A., Odom, S., Liao, K., Porter, F.D. and Rivera, J. (2006) Cholesterol deficiency in a mouse model of Smith–Lemli–Opitz syndrome reveals increased mast cell responsiveness. *J. Exp. Med.*, **203**, 1161–1171.
12. Wassif, C.A., Zhu, P., Kratz, L., Krakowiak, P.A., Battaile, K.P., Weight, F.F., Grinberg, A., Steiner, R.D., Nwokoro, N.A., Kelley, R.I. *et al.* (2001) Biochemical, phenotypic and neurophysiological characterization of a genetic mouse model of RSH/Smith–Lemli–Opitz syndrome. *Hum. Mol. Genet.*, **10**, 555–564.
13. Singh, P., Paila, Y.D. and Chattopadhyay, A. (2007) Differential effects of cholesterol and 7-dehydrocholesterol on the ligand binding activity of the hippocampal serotonin(1A) receptor: implications in SLOS. *Biochem. Biophys. Res. Commun.*, **358**, 495–499.
14. Porter, J.A., Young, K.E. and Beachy, P.A. (1996) Cholesterol modification of hedgehog signaling proteins in animal development. *Science*, **274**, 255–259.
15. Correa-Cerro, L.S., Wassif, C.A., Kratz, L., Miller, G.F., Munasinghe, J.P., Grinberg, A., Fliesler, S.J. and Porter, F.D. (2006) Development and characterization of a hypomorphic Smith–Lemli–Opitz syndrome mouse model and efficacy of simvastatin therapy. *Hum. Mol. Genet.*, **15**, 839–851.
16. Fitzky, B.U., Moebius, F.F., Asaoka, H., Waage-Baudet, H., Xu, L., Xu, G., Maeda, N., Kluckman, K., Hiller, S., Yu, H. *et al.* (2001) 7-Dehydrocholesterol-dependent proteolysis of HMG-CoA reductase suppresses sterol biosynthesis in a mouse model of Smith–Lemli–Opitz/RSH syndrome. *J. Clin. Invest.*, **108**, 905–915.
17. Lindegaard, M.L., Wassif, C.A., Vaisman, B., Amar, M., Wasmuth, E.V., Shamburek, R., Nielsen, L.B., Remaley, A.T. and Porter, F.D. (2008) Characterization of placental cholesterol transport: ABCA1 is a potential target for in utero therapy of Smith–Lemli–Opitz syndrome. *Hum. Mol. Genet.*, **17**, 3806–3813.
18. Tint, G.S., Yu, H., Shang, Q., Xu, G. and Patel, S.B. (2006) The use of the Dhcr7 knockout mouse to accurately determine the origin of fetal sterols. *J. Lipid Res.*, **47**, 1535–1541.
19. Sarmiere, P.D. and Bamburg, J.R. (2004) Regulation of the neuronal actin cytoskeleton by ADF/cofilin. *J. Neurobiol.*, **58**, 103–117.
20. Scott, R.W. and Olson, M.F. (2007) LIM kinases: function, regulation and association with human disease. *J. Mol. Med.*, **85**, 555–568.
21. van Galen, E.J. and Ramakers, G.J. (2005) Rho proteins, mental retardation and the neurobiological basis of intelligence. *Prog. Brain Res.*, **147**, 295–317.
22. Perkins, D.N., Pappin, D.J., Creasy, D.M. and Cottrell, J.S. (1999) Probability-based protein identification by searching sequence databases using mass spectrometry data. *Electrophoresis*, **20**, 3551–3567.
23. Newey, S.E., Velamoor, V., Govek, E.E. and Van Aelst, L. (2005) Rho GTPases, dendritic structure, and mental retardation. *J. Neurobiol.*, **64**, 58–74.
24. Kollins, K.M., Hu, J., Bridgman, P.C., Huang, Y.Q. and Gallo, G. (2009) Myosin-II negatively regulates minor process extension and the temporal development of neuronal polarity. *Dev. Neurobiol.*, **69**, 279–298.
25. Kubo, T., Endo, M., Hata, K., Taniguchi, J., Kitajo, K., Tomura, S., Yamaguchi, A., Mueller, B.K. and Yamashita, T. (2008) Myosin IIA is required for neurite outgrowth inhibition produced by repulsive guidance molecule. *J. Neurochem.*, **105**, 113–126.
26. Daub, H., Gevaert, K., Vandekerckhove, J., Sobel, A. and Hall, A. (2001) Rac/Cdc42 and p65PAK regulate the microtubule-destabilizing protein stathmin through phosphorylation at serine 16. *J. Biol. Chem.*, **276**, 1677–1680.
27. Krakowiak, P.A., Wassif, C.A., Kratz, L., Cozma, D., Kovarova, M., Harris, G., Grinberg, A., Yang, Y., Hunter, A.G., Tsokos, M. *et al.* (2003) Lathosterolosis: an inborn error of human and murine cholesterol synthesis due to lathosterol 5-desaturase deficiency. *Hum. Mol. Genet.*, **12**, 1631–1641.
28. Tierney, E., Nwokoro, N.A., Porter, F.D., Freund, L.S., Ghuman, J.K. and Kelley, R.I. (2001) Behavior phenotype in the RSH/Smith–Lemli–Opitz syndrome. *Am. J. Med. Genet.*, **98**, 191–200.
29. Sikora, D.M., Pettit-Kekel, K., Penfield, J., Merkens, L.S. and Steiner, R.D. (2006) The near universal presence of autism spectrum disorders in children with Smith–Lemli–Opitz syndrome. *Am. J. Med. Genet. A*, **140**, 1511–1518.
30. Bernard, O. (2007) Lim kinases, regulators of actin dynamics. *Int. J. Biochem. Cell Biol.*, **39**, 1071–1076.
31. Linseman, D.A. and Loucks, F.A. (2008) Diverse roles of Rho family GTPases in neuronal development, survival, and death. *Front Biosci.*, **13**, 657–676.
32. Luo, L. (2000) Rho GTPases in neuronal morphogenesis. *Nat. Rev. Neurosci.*, **1**, 173–180.
33. Pappu, A.S., Connor, W.E., Merkens, L.S., Jordan, J.M., Penfield, J.A., Illingworth, D.R. and Steiner, R.D. (2006) Increased nonsterol isoprenoids, dolichol and ubiquinone, in the Smith–Lemli–Opitz syndrome: effects of dietary cholesterol. *J. Lipid Res.*, **47**, 2789–2798.
34. Konstantinopoulos, P.A., Karamouzis, M.V. and Papavassiliou, A.G. (2007) Post-translational modifications and regulation of the RAS superfamily of GTPases as anticancer targets. *Nat. Rev. Drug Discov.*, **6**, 541–555.
35. Fong, L.G., Frost, D., Meta, M., Qiao, X., Yang, S.H., Coffinier, C. and Young, S.G. (2006) A protein farnesyltransferase inhibitor ameliorates disease in a mouse model of progeria. *Science*, **311**, 1621–1623.
36. Capell, B.C., Olive, M., Erdos, M.R., Cao, K., Faddah, D.A., Tavarez, U.L., Conneely, K.N., Qu, X., San, H., Ganesh, S.K. *et al.* (2008) A farnesyltransferase inhibitor prevents both the onset and late progression of cardiovascular disease in a progeria mouse model. *Proc. Natl Acad. Sci. USA*, **105**, 15902–15907.

37. Guirland, C., Suzuki, S., Kojima, M., Lu, B. and Zheng, J.Q. (2004) Lipid rafts mediate chemotropic guidance of nerve growth cones. *Neuron*, **42**, 51–62.
38. Labrador, J.P., Azcoitia, V., Tuckermann, J., Lin, C., Olaso, E., Manes, S., Bruckner, K., Goergen, J.L., Lemke, G., Yancopoulos, G. *et al.* (2001) The collagen receptor DDR2 regulates proliferation and its elimination leads to dwarfism. *EMBO Rep.*, **2**, 446–452.
39. Li, Z., Van Aelst, L. and Cline, H.T. (2000) Rho GTPases regulate distinct aspects of dendritic arbor growth in Xenopus central neurons *in vivo*. *Nat. Neurosci.*, **3**, 217–225.
40. Bergmann, C., Zerres, K., Senderek, J., Rudnik-Schoneborn, S., Eggermann, T., Hausler, M., Mull, M. and Ramaekers, V.T. (2003) Oligophrenin 1 (*OPHN1*) gene mutation causes syndromic X-linked mental retardation with epilepsy, rostral ventricular enlargement and cerebellar hypoplasia. *Brain*, **126**, 1537–1544.
41. Philip, N., Chabrol, B., Lossi, A.M., Cardoso, C., Guerrini, R., Dobyns, W.B., Raybaud, C. and Villard, L. (2003) Mutations in the oligophrenin-1 gene (*OPHN1*) cause X linked congenital cerebellar hypoplasia. *J. Med. Genet.*, **40**, 441–446.
42. Kutsche, K., Yntema, H., Brandt, A., Jantke, I., Nothwang, H.G., Orth, U., Boavida, M.G., David, D., Chelly, J., Fryns, J.P. *et al.* (2000) Mutations in ARHGEF6, encoding a guanine nucleotide exchange factor for Rho GTPases, in patients with X-linked mental retardation. *Nat. Genet.*, **26**, 247–250.
43. Pasteris, N.G., Cadle, A., Logie, L.J., Porteous, M.E., Schwartz, C.E., Stevenson, R.E., Glover, T.W., Wilroy, R.S. and Gorski, J.L. (1994) Isolation and characterization of the faciogenital dysplasia (Aarskog-Scott syndrome) gene: a putative Rho/Rac guanine nucleotide exchange factor. *Cell*, **79**, 669–678.
44. Schwartz, C.E., Gillessen-Kaesbach, G., May, M., Cappa, M., Gorski, J., Steindl, K. and Neri, G. (2000) Two novel mutations confirm FGD1 is responsible for the Aarskog syndrome. *Eur. J. Hum. Genet.*, **8**, 869–874.
45. Allen, K.M., Gleeson, J.G., Bagrodia, S., Partington, M.W., MacMillan, J.C., Cerione, R.A., Mulley, J.C. and Walsh, C.A. (1998) PAK3 mutation in nonsyndromic X-linked mental retardation. *Nat. Genet.*, **20**, 25–30.
46. Tassabehji, M., Metcalfe, K., Fergusson, W.D., Carette, M.J., Dore, J.K., Donnai, D., Read, A.P., Proschel, C., Gutowski, N.J., Mao, X. *et al.* (1996) LIM-kinase deleted in Williams syndrome. *Nat. Genet.*, **13**, 272–273.
47. Meng, Y., Zhang, Y., Tregoubov, V., Janus, C., Cruz, L., Jackson, M., Lu, W.Y., MacDonald, J.F., Wang, J.Y., Falls, D.L. *et al.* (2002) Abnormal spine morphology and enhanced LTP in LIMK-1 knockout mice. *Neuron*, **35**, 121–133.
48. Jiang, X.S., Tang, L.Y., Cao, X.J., Zhou, H., Xia, Q.C., Wu, J.R. and Zeng, R. (2005) Two-dimensional gel electrophoresis maps of the proteome and phosphoproteome of primitively cultured rat mesangial cells. *Electrophoresis*, **26**, 4540–4562.
49. Craig, R. and Beavis, R.C. (2003) A method for reducing the time required to match protein sequences with tandem mass spectra. *Rapid. Commun. Mass Spectrom.*, **17**, 2310–2316.
50. Keller, A., Nesvizhskii, A.I., Kolker, E. and Aebersold, R. (2002) Empirical statistical model to estimate the accuracy of peptide identifications made by MS/MS and database search. *Anal. Chem.*, **74**, 5383–5392.
51. Nesvizhskii, A.I., Keller, A., Kolker, E. and Aebersold, R. (2003) A statistical model for identifying proteins by tandem mass spectrometry. *Anal. Chem.*, **75**, 4646–4658.
52. Li, Z., Okamoto, K., Hayashi, Y. and Sheng, M. (2004) The importance of dendritic mitochondria in the morphogenesis and plasticity of spines and synapses. *Cell*, **119**, 873–887.